

Traveling strings of active dipolar colloids

Xichen Chao,¹ Katherine Skipper,² C. Patrick Royall,^{2,3} Silke Henkes,^{1,4} and Tanniemola B. Liverpool¹

¹*School of Mathematics, University of Bristol - Bristol BS8 1UG, UK*

²*H.H. Wills Physics Laboratory, Tyndall Avenue, Bristol, BS8 1TL, UK*

³*Gulliver UMR CNRS 7083, ESPCI Paris, Université PSL, 75005 Paris, France*

⁴*Lorentz Institute, LION, Leiden University - Leiden 2333 CA, NL*

(Dated: April 19, 2024)

We study an intriguing new type of self-assembled active colloidal polymer system in 3D. It is obtained from a suspension of Janus particles in an electric field that induces parallel dipoles in the particles as well as self-propulsion in the plane perpendicular to the field. At low packing fractions, in experiment, the particles self-assemble into 3D columns that are self-propelled in 2D. Explicit numerical simulations combining dipolar interactions and active self-propulsion find an activity dependent transition to a string phase by increasing dipole strength. We classify the collective dynamics of strings as a function of rotational and translational diffusion. Using an anisotropic version of the Rouse model of polymers with active driving, we analytically compute the strings' collective dynamics and centre of mass motion, which matches simulations and is consistent with experimental data. We also discover long range correlations of the fluctuations along the string contour that grow with the active persistence time, a purely active effect that disappears in the thermal limit.

Active matter describes a new class of materials that are composed of elements driven out of equilibrium by internal sources of energy. These systems promise a novel way to add functionality in materials design for a variety of applications, from drug delivery to metamaterials [1–7]. A major challenge however is how to *control* activity, i.e. which components of a system are active, when that activity is to be switched on/off, and how to use it to steer emergent collective behaviour towards a desired function. One promising avenue for controlling active matter is by tuning the interplay between active driving and passive mechanics of the mesoscale structures of the active material at scales intermediate between the microscopic building blocks and the macroscopic (hydrodynamic) scales [8]. This dynamic structure at the mesoscale can take the form of polymers [9–12], membranes [13], and disordered or ordered solids [14–17]. Because of the complex internal dynamics of these mesostructures, more detailed descriptions, going beyond long wavelength hydrodynamics, must be developed to precisely uncover the physical principles required to accurately control their behaviour.

Extended one-dimensional polymeric structures are a promising mesoscale ingredient as their relatively open structure leaves the system more susceptible to external controls. Hence there has been a corresponding resurgence of experimental and theoretical work on active polymer systems [18–20]. Most experimental realisations of active polymer systems have been biological, e.g. motor-driven cytoskeletal polymers [21] or living organisms such as worms [19]. Theoretical studies have included tangentially driven linear polymers and ring polymers, mostly in 2D [20, 22–24] and more recently have begun to look at entanglement [25]. Biological components however are hard to control and there is a need for systems built from man-made (synthetic) components.

Active Janus colloids are one of the simplest experimental building blocks of synthetic active materials – their single particle dynamics is reasonably well approximated by active Brownian particles [26–28]. The Janus particles of interest here are made from an insulating colloid half coated by metal which is itself then coated in a layer of insulator. When placed in an oscillating electric field, by the process of induced-charge electrophoresis (ICEO) [29, 30], they simultaneously become active and interact via pairwise dipolar interactions. The colloids undergo sedimentation to the bottom of the sample. Hence they can self-assemble on the bottom surface into 2D polymer-like motile chains [31–33]. Recent experiments have shown however that it is possible to study this system in fully 3D by suspending smaller Janus particles in a solvent, which due to their size sediment markedly less [34]. At low volume fractions, the particles self-assemble into active columns (strings) that self-propel in the plane perpendicular to their axis. We note it is well known from experiments [35, 36] and simulations [37] that a passive collection of suspended dipolar colloids have a *static* string phase at low density.

In this letter, we study the collective dynamics of the low density phase of actively travelling strings through a combination of numerical simulations, theoretical tools, and experimental analysis. Our numerical model combines short range repulsion, dipolar interactions in the direction of the field and self propulsion, and we find an activity-dependent transition to the active string phase as a function of dipole strength. We explore the collective dynamics of strings as a function of rotational and translational diffusion strengths. Using a generalised Rouse model of anisotropic 3-dimensional flexible polymers with active driving allows us to capture the string dynamics. In addition to explaining the global string dynamics, this predicts a purely active emergent correlation length

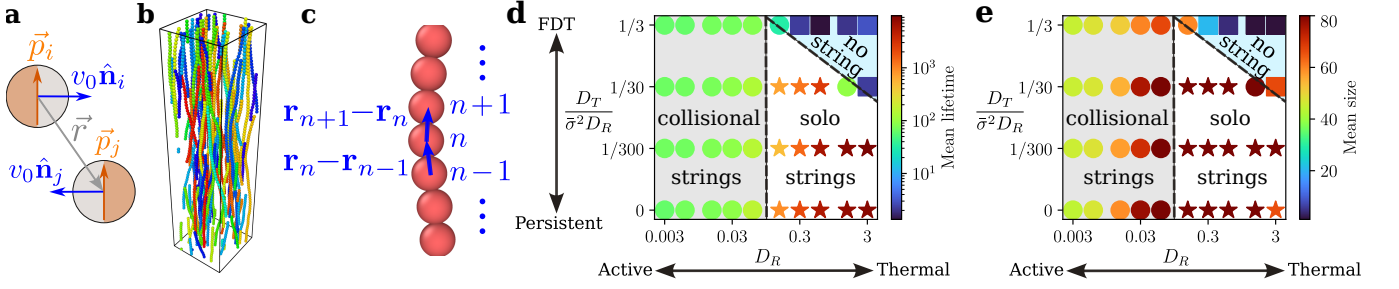


FIG. 1. **a** - Schematic of the Janus particle used in experiments. The dipoles $\mathbf{p}_i = (0, 0, p)$ are aligned with electric field direction and perpendicular to self-propelling velocities $\mathbf{v}_0 = v_0(\cos \theta_i, \sin \theta_i, 0)$. $\mathbf{r} = (x, y, z)$ is the vector separating the positions of two bead centres. **b** - Simulations conducted in LAMMPS and visualised in OVITO [38], with packing fraction 5%. Different colors indicate different clusters. **c** - The bond vector for a single string, with \mathbf{r}_n the position of the n th bead. **d-e**, Phase diagrams of the mean lifetime and mean size of traveling strings. $p = 1, v_0 = 0.5$ as a function of rotational diffusion coefficient D_R and ratio $\frac{D_T}{\sigma^2 D_R}$. The three regimes and markers in these phase diagrams are determined by the mean lifetime phase diagram. The colourbar in the mean size phase diagram is linear and is logarithmic in the mean lifetime phase diagram. These phase diagrams are based on simulations with box size $20 \times 20 \times 80$.

along the strings. We further carry out experiments with metallo-silica Janus particles that we study with confocal microscopy at the single-particle level [39]. We verify that our theoretical model agrees very well with simulations and is consistent with experiments.

Simulation — We model our dipolar active colloids by adopting a hybrid potential that combines the Weeks-Chandler-Anderson (WCA) potential for short-range repulsive interactions between particles with a dipole-dipole (DD) pair interaction that accounts for the long-range dipolar forces present in the system [37]. In experiment, the dipole moments are aligned with the oscillating electric field $\mathbf{E} = E\hat{z}$ [32, 34]. Hence all particles have a constant identical dipole moment $\mathbf{p} = p\hat{z}$ with dipole strength p (that increases with $|E|$). The interaction potential between particles i and j , is $U_{HY,ij} = U_{WCA}(r_{ij}) + U_{DD}(\mathbf{p}, r_{ij})$ with

$$U_{WCA}(r) = 4\epsilon \left[\left(\frac{\sigma}{r} \right)^{12} - \left(\frac{\sigma}{r} \right)^6 \right], \quad r < 2^{1/6}\sigma, \quad (1)$$

$$U_{DD}(\mathbf{p}, r) = \frac{1}{r^3}(\mathbf{p} \cdot \mathbf{p}) - \frac{3}{r^5}(\mathbf{p} \cdot \mathbf{r})(\mathbf{p} \cdot \mathbf{r}),$$

where $\mathbf{r}_{ij} = \mathbf{r}_i - \mathbf{r}_j$ is the inter-particle separation and $r_{ij} = |\mathbf{r}_{ij}|$. We choose units such that the WCA potential strength $\epsilon = 1$ and the particle diameter is $\bar{\sigma} = 2^{1/6}\sigma = 1$. The DD pair interaction is attractive along the direction of the polarisation \mathbf{p} and repulsive in the orthogonal plane, naturally leading to the formation of parallel strings along \hat{z} . Due to ICEO, each Janus particle rotates until the interface between the two halves is parallel to \mathbf{E} , and therefore self-propels in a direction in the xy plane (Fig. 1a). The Debye screening length in experiment is much smaller than particle diameter, allowing us to cut off dipole interactions after the first neighbour for computational efficiency.

We combine $U_{HY,ij}$ with overdamped Active Brownian

dynamics without hydrodynamics,

$$\dot{\mathbf{r}}_i = -\frac{1}{\zeta} \sum_{j \neq i} \nabla_i U_{HY,ij} + v_0 \hat{\mathbf{n}}_i + \boldsymbol{\eta}_i^T, \quad (2)$$

$$\dot{\hat{\mathbf{n}}}_i = (\cos \theta_i, \sin \theta_i, 0), \quad \dot{\theta}_i = \eta_i^R,$$

where $\{\mathbf{r}_i, \theta_i\}$ are the position, orientation of the i th particle and ζ is the Stokes drag. We include activity with self-propulsion speed v_0 (that in experiment increases with $|E|$) in the direction $\hat{\mathbf{n}}_i$, which is constrained to the xy plane, orthogonal to \hat{z} (Fig. 1a). Its in-plane angle θ_i diffuses with rotational white noise η_i^R , with correlation $\langle \eta_i^R(t) \eta_m^R(t') \rangle = 2D_R \delta(t - t') \delta_{nm}$, where D_R is the rotational diffusion coefficient. We also include translational white noise $\boldsymbol{\eta}_i^T$ in all directions, with correlations $\langle \eta_{\alpha n}^T(t) \eta_{\beta m}^T(t') \rangle = 2D_T \delta(t - t') \delta_{\alpha\beta} \delta_{nm}$ where D_T is the translational diffusion coefficient. The simulation box is periodic in all three dimensions and we use LAMMPS [40] with a custom ABP integrator [41].

In our simulations, we systematically vary the dipole strength, speed and diffusion coefficients via the parameters $(p, v_0, D_R, \frac{D_T}{\sigma^2 D_R})$ while maintaining a fixed low packing fraction $\phi = 0.05$. Strings are defined by a clustering algorithm with neighbour cutoff distance $1.05\bar{\sigma}$ (Fig. 1b). Here we first locate the transition to the string phase by varying p and v_0 independently for intermediate $D_R = 0.15$ and different D_T (Fig. S2.1a-d). The transition from a disordered phase at low p to a string phase at high p shifts from around $p = 0.2 - 0.3$ at $v_0 = 0.1$ to $p \lesssim 1$ at $v_0 = 0.7$. We choose the point $p = 1$ and $v_0 = 0.5$, which is in the string phase in almost all cases. We find that string formation is subject to slow coarsening dynamics, necessitating runs of $t = 20000$ time units to reach steady-state (Fig. S2.2a). Strings also rapidly lengthen when p increases (Fig. S2.2b), and we switch to a tall simulation box $L_x \times L_y \times L_z \equiv 20 \times 20 \times 80$ for our main runs (Fig. 1b). Strings can still span the system, so we cut off string size at $L_z/\bar{\sigma} = 80$.

The persistence of active driving is regulated by rotational diffusion, D_R and translational diffusion, D_T . If the fluctuation-dissipation theorem (FDT) holds, $D_T = k_B T / \zeta$ and $D_R = k_B T / \zeta_r$. For Stokes drag, where $\bar{\sigma}^2 \zeta = 3\zeta_r$, this implies that $\frac{D_T}{\bar{\sigma}^2 D_R} = \frac{1}{3}$ in simulation units. Another limit, considered in many ABP simulations is where orientational noise dominates and one can set $D_T \approx 0$ (“persistent”). Finally when D_R is very large the effect of activity is to give an effectively thermal system with a renormalized *active temperature* (“thermal”). The two axes of our phase diagrams are then D_R and $\frac{D_T}{\bar{\sigma}^2 D_R}$, with D_R varying from 0.003 to 3, which correspond to an active limit and a thermal limit respectively. $\frac{D_T}{\bar{\sigma}^2 D_R}$ varies from 0 to $\frac{1}{3}$, which indicate a persistent limit and the FDT limit, respectively. With this parameter scan, we construct a phase diagram that focuses on *active* string dynamics (Fig. 1d-e). We measure the mean size and mean lifetime of strings, defined as time interval between changes in string composition. With the exception of a string-less phase at high D_R and D_T , i.e. a thermal FDT limit, the value of D_R predicts string properties. We find a phase of medium-sized strings that interact through *collisions* with lifetimes $\tau_l \sim 100$ when D_R is relatively low ($D_R \leq 0.06$) and a phase of non-interacting *solo* strings with rapidly increasing τ_l and lengths that exceed the system size and wrap the box when $D_R \geq 0.15$. We return to this characterisation below.

We probe the collective motion of traveling strings, first focusing on the motion of their centroids. We fit the mean square displacement (MSD) of the centroids of the strings in the xy plane to the MSD of a free 2-dimensional (2D) ABP in the absence of pair interactions [42, 43]. The effective translational diffusion coefficient of centroids decays with string length as $D_c \sim N^{-1}$, whereas the collective self-propulsion speed decays with the square root of length $v_c \sim N^{-1/2}$ (Fig. 2), and both are independent of dipole strength p , and phase.

Active Anisotropic Rouse model — We can gain an understanding of string dynamics by mapping a single string to an active polymer model. By solving $\nabla U_{HY}(\mathbf{r}) = 0$, we find the equilibrium distance between two particles $a(p)$, which is a function of the dipole strength p . By expanding the hybrid potential U_{HY} near its stable equilibrium position $\mathbf{r}^{(0)}$, we can obtain an effective elastic potential $U_E := \frac{1}{2}(\mathbf{r} - \mathbf{r}^{(0)}) \cdot \mathbf{H}_U(\mathbf{r}^{(0)}) \cdot (\mathbf{r} - \mathbf{r}^{(0)})^T$, with \mathbf{H}_U the Hessian matrix. \mathbf{H}_U is diagonal and our three effective elastic constants are given by $\kappa_{11}(p) := \left. \frac{\partial^2 U_{HY}}{\partial x^2} \right|_{\mathbf{r}=\mathbf{r}^{(0)}} = \left. \frac{\partial^2 U_{HY}}{\partial y^2} \right|_{\mathbf{r}=\mathbf{r}^{(0)}}$ and $\kappa_{33}(p) := \left. \frac{\partial^2 U_{HY}}{\partial z^2} \right|_{\mathbf{r}=\mathbf{r}^{(0)}}$. These elastic constants are functions of the dipole strength p and are isotropic in the xy plane. $\kappa_{11}(p)$ and $\kappa_{33}(p)$ are both strongly increasing with p , and $\kappa_{33} \gg \kappa_{11}$. See SI section 3.1 for details.

For a string of size N , the position of the n th particle can be expanded around a rigid column as $\mathbf{r}_n :=$

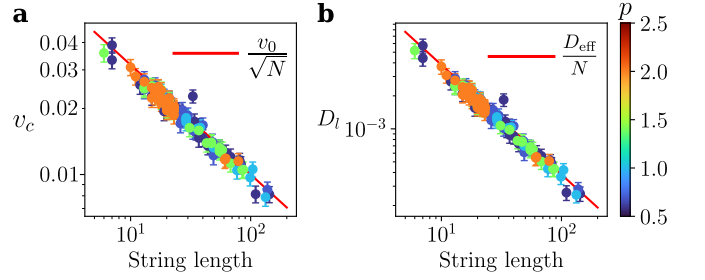


FIG. 2. Collective dynamics of traveling strings as a function of their length. **a** - Self-propulsion speed of string centroids v_c and **b** - Collective long-time translational diffusion coefficient D_l (see Eqn. (4)). The two red lines are our theoretical predictions Eqn. 4. Data is extracted from simulations at $v_0 = 0.1, D_R = 0.15, \frac{D_T}{\bar{\sigma}^2 D_R} = \frac{1}{30}, p \in [0.6, 0.7, 1.0, 1.4, 2.0]$, with colorbars indicating dipole strength p . Error bars correspond to the standard deviation of the fit. The D_l data are obtained from v_c and D_c (Fig. S2.2); v_c dominates D_l in this regime resulting in similar plot shapes. Error was propagated by assuming independent normal distributions. All data is picked from the last 5000 time units in steady state.

$\mathbf{r}_n^{(0)} + \mathbf{R}_n$ where $\mathbf{r}_n^{(0)} = (0, 0, an)$ and fluctuations $\mathbf{R}_n = (R_{1n}, R_{2n}, R_{3n}) := (x_n, y_n, z_n), 1 \leq n \leq N$ (Fig. 1c). The equations of motion for the strings therefore are an active anisotropic Rouse model [44] (see SI section 3.2),

$$\begin{aligned} \dot{R}_{\alpha n} &= \frac{\kappa_{\alpha\alpha}}{\zeta} \frac{\partial^2 R_{\alpha n}}{\partial n^2} + A_{\alpha n} + \eta_{\alpha n}^T, \\ \dot{\theta}_n &= \eta_n^R. \end{aligned} \quad (3)$$

for $\alpha = 1, 2, 3$. Here activity $\mathbf{A}_n = (A_{1n}, A_{2n}, A_{3n})$ is confined to the xy plane, i.e. $A_{1n} = v_0 \cos \theta_n$, $A_{2n} = v_0 \sin \theta_n$ and $A_{3n} = 0$. Using Rouse modes [22, 44], the equations can be solved analytically and various collective quantities obtained. Please see SI section 3.2-3.3 for details.

The motion of the centroid of the string is given by the lowest (0th) Rouse mode. We therefore compute the MSD of the string centroid in the xy plane to obtain $\text{MSD}_{\text{string}} = 4D_c t + 2v_c^2 D_R^{-1} [t + D_R^{-1} (e^{-D_R t} - 1)]$, with an effective translational diffusion coefficient D_c and the collective self-propulsion speed v_c . Comparing the collective $\text{MSD}_{\text{string}}$ with that of a single ABP [42, 43], we find

$$v_c = \frac{v_0}{\sqrt{N}}, \quad D_c = \frac{D_T}{N}, \quad D_l = D_c + \frac{v_c^2}{2D_R} = \frac{D_{\text{eff}}}{N}. \quad (4)$$

We also obtain D_l , the long-time diffusion coefficient of string centroids in terms of $D_{\text{eff}} = D_T + v_0^2 / (2D_R)$, the long-time diffusion coefficient of an isolated Janus colloid with both translational noise and active driving. Our result also shows that the persistence time of the strings D_R^{-1} is the same as that of a single particle. Hence, we find the collective dynamics of traveling strings is solely governed by their length and Eqn. 4 accurately predicts the simulation results (red lines in Fig. 2).

We can understand the difference between *collisional* and *solo* strings with this simple argument: for fixed average string size $\langle N \rangle$, in the low D_R (collisional) limit, strings move persistently for their mean free path [45] which can be approximated as $l_f \approx \frac{\pi \langle N \rangle \bar{\sigma}^3}{12 R L_z \phi}$, where R is the xy radius of gyration, and $\frac{6 L_z \phi}{\pi \langle N \rangle \bar{\sigma}^3}$ the projected $2d$ density of strings, leading to an approximate lifetime $\tau_l^{\text{coll}} \approx l_f / v_c$. In contrast, in the solo regime with large D_R , they are moving diffusively and traverse this distance in $\tau_l^{\text{diff}} \approx \frac{l_f^2}{4 D_l} \gg \tau_l^{\text{coll}}$, leading to a much longer lifetime. Using $\langle N \rangle = 80, L_z = 80 \bar{\sigma}$ and $R = 1.5$, this is a good match for the observed string life times at low $\frac{D_T}{\bar{\sigma}^2 D_R}$ (see Fig. S2.3).

In addition to their persistent centroid motion, the fluctuations along the strings are also highly spatially correlated (Fig. 1b and SI movies). These mesoscale spatial correlations emerge from the temporal correlations of the active driving coupling preferentially to the long wavelength elastic modes [14, 15].

To illustrate this, we analyse the correlations of the *bond-vectors*, i.e $\mathbf{b}_n = \mathbf{r}_n - \mathbf{r}_{n-1}$, at different positions on the traveling strings (see Fig. 1c). We find new active contributions which are due to the finite time correlations in the directions of local active driving. The relevant correlation function is the correlation between the *deviations* of the bonds from those of a rigid column: $\mathbf{B}_n = \mathbf{R}_n - \mathbf{R}_{n-1} = \mathbf{b}_n - (0, 0, a)$. We obtain an exact expression for this bond-vector deviation correlation function, $C_t(n, n') = \langle \mathbf{B}_n \cdot \mathbf{B}_{n'} \rangle$, using the higher Rouse modes (see SI section 3.5): $C_t(n, n) = \frac{2aD_a}{\xi D_R} \left(e^{-\frac{a}{\xi}} - 1 \right) + 2\zeta \left(\frac{D_T + D_a}{\kappa_{11}} + \frac{D_T}{2\kappa_{33}} \right) := C_{t0}$ when $n = n'$, and

$$C_t(n, n') = \frac{aD_a}{\xi D_R} \left(e^{\frac{a}{\xi}} + e^{-\frac{a}{\xi}} - 2 \right) e^{-\frac{a}{\xi} |n - n'|}, \quad (5)$$

which is valid when the bonds are far from the ends, $1 \ll n \neq n' \ll N$. Here $D_a = \frac{v_0^2}{2D_R}$ is the active contribution to the ABP effective translational diffusion coefficient. The correlation length $\xi = a \sqrt{\frac{\kappa_{11}}{D_R \zeta}}$ of the exponential decay scales as $\frac{1}{\sqrt{D_R}}$, i.e. with the square root of active persistence time (Fig. 3a). We note that in the thermal limit, the system is a flexible chain with no bond vector correlations when $n \neq n'$, i.e. the correlations are a purely active effect. Fig. 3b shows how in the thermal limit $D_R \rightarrow \infty$, the $n = n'$ part of C_t decays to a constant proportional to D_T , whereas for $|n - n'| \neq 0$ it decays to 0. Eqn. 5 is an excellent match to simulations of an isolated (non-interacting) string system over several D_R (see Fig. 3c). In the simulations we have subtracted the mean squared equilibrium distance between two consecutive particles, a^2 from $\langle \mathbf{b}_n \cdot \mathbf{b}_{n'} \rangle$. For interacting strings (see Fig. 3d), there is still excellent agreement if we modify the reference state for the bond deviations: $\mathbf{B}_n = \mathbf{b}_n - (0, 0, a_{em})$, with a_{em} determined by an empir-

ical least squares fit. In Fig. S2.4, we show correlations for a range of D_R and the best fit a_{em}/a .

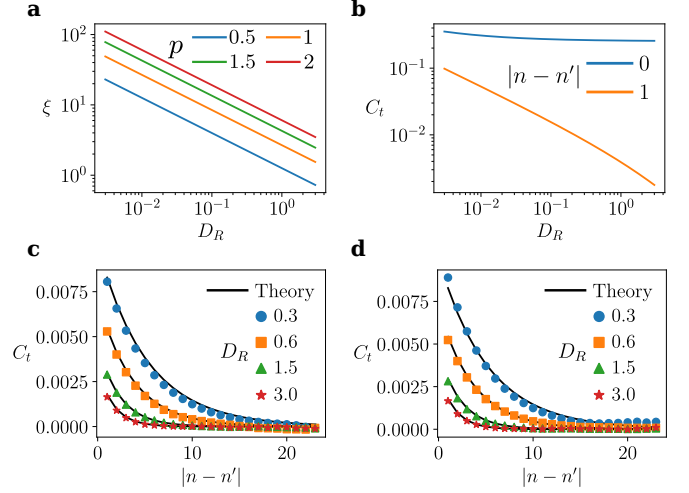


FIG. 3. **a** - Correlation length $\xi \sim D_R^{-1/2}$ for different dipole strengths p . **b** - Theoretical C_t at $|n - n'| = 0, 1$. **c-d**, Bond vector correlation functions in non-interacting (**c**) and interacting (**d**) string systems. $p = 1, v_0 = 0.5, \frac{D_T}{\bar{\sigma}^2 D_R} = \frac{1}{300}$. Points are simulation data, lines are theoretical predictions.

Experiment — In our experiments, we use the 3D induced-charge electrophoresis system previously developed by one of us [34]. Janus particles made from an insulating colloid half coated by metal are placed in an oscillating electric field E . We study a fixed volume fraction of 5%. In this system, the Janus colloids move like active Brownian particles in a plane orthogonal to the field (xy) and diffuse in the third direction (z). Due to the imbalance of the dielectric constant between the solvent and the particles, dipolar interactions are induced by the external electric field, which point in the direction of the field. For our parameters (5 kHz and NaCl at a concentration of $10^{-4} \text{ mol} \cdot \text{L}^{-1}$, i.e. 0.1mM), the interactions between the particles can be approximated as a single effective dipole located at the centre. The Debye screening length is $\approx 26 \text{ nm}$. Here we focus on experiments with an external electric field amplitude $E = \frac{1}{3} \text{ V}/\mu\text{m}$ at 5KHz frequency, giving us an individual particle Péclet number $\text{Pe} \approx 40$. Due to limited z resolution, we use Trackpy to first identify particles with good xy accuracy in individual z layers vertically spaced by $a_{\text{eff}} = 2.6 \mu\text{m}$, the effective particle spacing at this salt concentration.

We find a landscape of cairn-like strings [46] (columns) with variable height growing from the bottom surface, due to the finite gravitational length (Fig. 4a). To identify strings, we developed a clustering algorithm that follows strings from the top to the bottom by connecting to the nearest point, if any, within a_{eff} . Due to the finite scan-time for each z -layer, moving from the bottom to the top of the image *and* the fact that the strings are self-propelled, moving with instantaneous velocity \mathbf{v} in

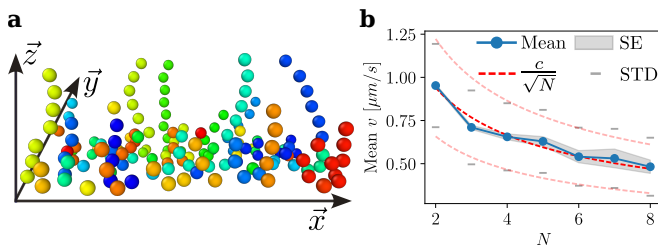


FIG. 4. **a** - Coordinates from experimental data. Different colors indicate different strings. **b** - Mean instantaneous speed plot. We average the speed over strings of the same length. The best fit of the mean is $v = \frac{c}{\sqrt{N}}$ with $c = 1.3$. The gray bars indicate the standard deviation and the shaded area is the standard error of the mean.

the xy -plane, the observed strings appear tilted. If the scan time of the string τ_s is less than D_R^{-1} , the string approximately travels in a fixed direction during the scan (we estimate $\tau_s \lesssim D_R^{-1}$). We can then measure the velocity \mathbf{v} of traveling strings from the tilt angle (and plane) of the strings. We perform a least-squares analysis on the beads in the string to obtain a best fit straight line, l_s making an angle θ_s with $\hat{\mathbf{z}} = (0, 0, 1)$. ($\theta_s < \frac{\pi}{2}$). If in a time τ_s , the camera has scanned up to height z_s , then the string angle θ_s and its instantaneous speed $v = |\mathbf{v}|$ are related by $v\tau_s = \tan \theta_s z_s$. Using our imaging parameters, we find $v = 1.5802 \tan \theta_s \mu\text{ms}^{-1}$ in our experiment. By averaging v over strings with the same length N we find that the mean v decays with N as $\frac{1}{\sqrt{N}}$ (Fig. 4b), which is consistent with our simulations and theory.

In conclusion, we have studied a string forming 3D active dipolar colloidal system using simulations, theory and experiment. The collective dynamics of traveling strings, derived analytically and confirmed by numerical simulations and experimental analyses, has a simple dependence on string length. At low packing fractions, the string dynamics is well described by an active anisotropic Rouse model, showing emergent active bond vector correlations. In future work we plan to extend our analysis to the active sheets and labyrinth appearing at higher packing fractions [34], where we also expect additional hydrodynamic contributions to string dynamics.

The authors would like to thank the Isaac Newton Institute for Mathematical Sciences, Cambridge, for support and hospitality during the programme *New statistical physics in living matter*, where part of the work on this paper was undertaken. This work was supported by EPSRC grants EP/R014604/1 and EP/T031077/1. X.C. is supported by Bristol-CSC joint program.

[1] J. R. Baylis, J. H. Yeon, M. H. Thomson, A. Kazerooni, X. Wang, A. E. St. John, E. B. Lim, D. Chien, A. Lee, J. Q. Zhang, *et al.*, Science advances **1**, e1500379 (2015).

[2] R. Di Leonardo, L. Angelani, D. Dell’Arciprete, G. Ruocco, V. Iebba, S. Schippa, M. P. Conte, F. Mecarini, F. De Angelis, and E. Di Fabrizio, Proceedings of the National Academy of Sciences **107**, 9541 (2010).

[3] S. Krishnamurthy, S. Ghosh, D. Chatterji, R. Ganapathy, and A. Sood, Nature Physics **12**, 1134 (2016).

[4] J. Stenhammar, R. Wittkowski, D. Marenduzzo, and M. E. Cates, Science advances **2**, e1501850 (2016).

[5] G. Frangipane, D. Dell’Arciprete, S. Petracchini, C. Maggi, F. Saglimbeni, S. Bianchi, G. Vizsnyiczai, M. L. Bernardini, and R. Di Leonardo, Elife **7**, e36608 (2018).

[6] J. Arlt, V. A. Martinez, A. Dawson, T. Pilizota, and W. C. Poon, Nature communications **9**, 768 (2018).

[7] Y. Chen, X. Li, C. Scheibner, V. Vitelli, and G. Huang, Nature communications **12**, 5935 (2021).

[8] M. C. Marchetti, J.-F. Joanny, S. Ramaswamy, T. B. Liverpool, J. Prost, M. Rao, and R. A. Simha, Reviews of modern physics **85**, 1143 (2013).

[9] D. Humphrey, C. Duggan, D. Saha, D. Smith, and J. Käs, Nature **416**, 413 (2002).

[10] T. Liverpool, A. Maggs, and A. Ajdari, Physical review letters **86**, 4171 (2001).

[11] T. Eisenstecken, G. Gompper, and R. G. Winkler, Polymers **8**, 304 (2016).

[12] B. Chakrabarti, Y. Liu, J. LaGrone, R. Cortez, L. Fauci, O. Du Roure, D. Saintillan, and A. Lindner, Nature Physics **16**, 689 (2020).

[13] S. C. Al-Izzi, P. Sens, M. S. Turner, and S. Komura, Soft Matter **16**, 9319 (2020).

[14] S. Henkes, K. Kostanjevec, J. M. Collinson, R. Sknepnek, and E. Bertin, Nature communications **11**, 1405 (2020).

[15] L. Caprini, U. M. B. Marconi, and A. Puglisi, Physical review letters **124**, 078001 (2020).

[16] T. H. Tan, A. Mietke, J. Li, Y. Chen, H. Higinbotham, P. J. Foster, S. Gokhale, J. Dunkel, and N. Fakhri, Nature **607**, 287 (2022).

[17] C. Scheibner, A. Souslov, D. Banerjee, P. Surówka, W. T. Irvine, and V. Vitelli, Nature Physics **16**, 475 (2020).

[18] V. Schaller, C. Weber, C. Semmrich, E. Frey, and A. R. Bausch, Nature **467**, 73 (2010).

[19] A. Deblais, K. Prathyusha, R. Sinaasappel, H. Tuazon, I. Tiwari, V. P. Patil, and M. S. Bhamla, Soft Matter **19**, 7057 (2023).

[20] M. Fazelzadeh, E. Irani, Z. Mokhtari, and S. Jabbari-Farouji, Physical Review E **108**, 024606 (2023).

[21] D. Mizuno, C. Tardin, C. F. Schmidt, and F. C. MacKintosh, Science **315**, 370 (2007).

[22] T. Liverpool, Physical Review E **67**, 1 (2003).

[23] R. E. Isele-Holder, J. Elgeti, and G. Gompper, Soft matter **11**, 7181 (2015).

[24] K. Prathyusha, S. Henkes, and R. Sknepnek, Physical Review E **97**, 022606 (2018).

[25] S. Mandal, C. Kurzthaler, T. Franosch, and H. Löwen, Physical Review Letters **125**, 138002 (2020).

[26] M. C. Marchetti, Y. Fily, S. Henkes, A. Patch, and D. Yllanes, Current Opinion in Colloid & Interface Science **21**, 34 (2016).

[27] C. Bechinger, R. Di Leonardo, H. Löwen, C. Reichhardt, G. Volpe, and G. Volpe, Reviews of Modern Physics **88**, 045006 (2016).

[28] M. E. Cates and J. Tailleur, Annu. Rev. Condens. Matter Phys. **6**, 219 (2015).

- [29] T. M. Squires and M. Z. Bazant, *Journal of Fluid Mechanics* **560**, 65 (2006).
- [30] S. Gangwal, O. J. Cayre, M. Z. Bazant, and O. D. Velev, *Physical review letters* **100**, 058302 (2008).
- [31] A. E. Patteson, A. Gopinath, and P. E. Arratia, *Current Opinion in Colloid & Interface Science* **21**, 86 (2016).
- [32] J. Yan, M. Han, J. Zhang, C. Xu, E. Luijten, and S. Granick, *Nature materials* **15**, 1095 (2016).
- [33] J. Zhang, R. Alert, J. Yan, N. S. Wingreen, and S. Granick, *Nature Physics* **17**, 961 (2021).
- [34] N. Sakaï and C. P. Royall, *arXiv preprint arXiv:2010.03925* (2020).
- [35] R. Tao, *Journal of Physics: Condensed Matter* **13**, R979 (2001).
- [36] A. Yethiraj and A. Van Blaaderen, *Nature* **421**, 513 (2003).
- [37] A.-P. Hynninen and M. Dijkstra, *Physical review letters* **94**, 138303 (2005).
- [38] A. Stukowski, *Modelling and simulation in materials science and engineering* **18**, 015012 (2009).
- [39] A. Ivlev, G. Morfill, H. Lowen, and C. P. Royall, *Complex plasmas and colloidal dispersions: particle-resolved studies of classical liquids and solids*, Vol. 5 (World Scientific Publishing Company, 2012).
- [40] A. P. Thompson, H. M. Aktulga, R. Berger, D. S. Bolintineanu, W. M. Brown, P. S. Crozier, P. J. In't Veld, A. Kohlmeyer, S. G. Moore, T. D. Nguyen, *et al.*, *Computer Physics Communications* **271**, 108171 (2022).
- [41] S. Cameron, M. Mosayebi, R. Bennett, and T. B. Liverpool, *Physical Review E* **108**, 014608 (2023).
- [42] J. R. Howse, R. A. Jones, A. J. Ryan, T. Gough, R. Vafabakhsh, and R. Golestanian, *Physical review letters* **99**, 048102 (2007).
- [43] D. Breoni, M. Schmiedeberg, and H. Löwen, *Physical Review E* **102**, 062604 (2020).
- [44] M. Doi, S. F. Edwards, and S. F. Edwards, *The theory of polymer dynamics*, Vol. 73 (oxford university press, 1988).
- [45] P. M. Chaikin and T. C. Lubensky, *Principles of Condensed Matter Physics* (Cambridge University Press, Cambridge, 1995).
- [46] <https://en.wikipedia.org/wiki/Cairn>.